Periodica Polytechnica
Transportation Engineering

46(2), pp. 82-94, 2018
https://doi.org/10.3311/PPtr.11491

Introduction of a Cost Effective Method for Analysing Engine Intake Ice Removal Device for Small Aircraft

György Bicsák[1*], Árpád Veress[1], Máté Erdősi[2], Vítězslav Hanzal[3]

RESEARCH ARTICLE

Received 23 March 2017; accepted 20 September 2017

Abstract

As the need for personal air transport increases significantly, new aircraft and/or its components are required to be designed and developed together with expectations for guarantying the high level flight safety. Since smaller aircraft manufacturers don't have the infrastructural and experimental resources for complex investigations, analysis of engine components with especial care for the behaviour of particle separation components in the inlet air duct for example, smarter, more efficient solutions have to be developed. CFD software gives an opportunity to simulate the trajectories of different type of particles, such as hailstones, dust, or even liquid water droplets. Hence, in this study an upper-wing type, two engines thrusted, small turboprop aircraft's integrated engine air intake device has been analysed, to prove the effectivity of the aircraft performance in the considered raining and icing conditions. The flow field has been discretized with a detailed, hybrid mesh using hexa elements at the simpler parts, and tetra elements, where the geometry is more complex. Inflation layers have been inserted on the wall-type surfaces, with especial care to the problematic parts, where the y+ number is predictably higher. The inlet boundary conditions of the model have been extracted from a larger, complex pre-simulation, performed in a previous study. Standard Reynolds Averaged Navier-Stokes equations have been considered with Shear Stress Transport turbulence model. Solid (ice) and liquid particles have been defined, and their trajectories are investigated by using fully coupled model. The interaction of the wall-fluid particle has been taken into consideration.

Keywords

CFD, particle tracking, Lagrangian particle transport modelling, particle and ice remover device

[1] Department of Aeronautics, Naval Architecture and Railway Vehicles, Faculty of Transportation Engineering and Vehicle Engineering, Budapest University of Technology and Economics, H-1111 Budapest, Műegyetem rkp. 3., Hungary

[2] Knorr-Bremse & Center Budapest, Engineering Calculation Group, H-1111 Budapest, Major u. 69, Hungary

[3] VZLU Aerospace Research & Test Establishment, Beranovych 130, CZ-19905 Prague - Letnany, Czech Republic

[*] Corresponding author, e-mail: gybicsak@vrht.bme.hu

1 Introduction

The need for different calculation methods is increased significantly due to the highly cost efficient solutions. Several researches (Hargitai, 2012; Beneda, 2008) were in line with these approaches in the vehicle engineering in the last decade. Furthermore, regarding the aeronautical sector, as air traffic continuously increases; it has become essential to ensure the maximum flight safety (Rohács, 2015) beside expected performance and efficiency with including the application of optimization (Hanzal, 2015). Consequently while for larger manufacturers there are enormous power and human resource capacity, and different developments are supported by highly utilized simulation tools and test benches, for smaller aircraft developers, manufacturers the available resources are usually limited. Several international projects target these companies to ensure the "know-how" for these contributors, such as the ESPOSA project. Hence, in line with these efforts, the main goal of the present paper is to introduce a cost efficient calculation method for modelling and simulating particle filtering by engine intake ice remover device with especial care for the water droplets and ice particles.

The particle tracking, particle separation is a significant research field; many publications are available in this area. Different types of solid or fluid particles can cause problems in turbomachinery (Brun et al., 2012). Several separation techniques and/or methods are available in aerospace (Musgrove et al., 2009; Bojdo and Filippone, 2011), vehicle applications (Lindberg, 2015) or even in food processing (Anandharamakrishnan, 2013). Depending on the problem, some effects can be neglected from the calculation; but others, as gravitation, viscosity or electromagnetics have considerably high effect (Hellmann et al., 2014). The simulation of particle tracking for positron emission (Chang et al., 2013) or cells and low sized particles (Meijering et al., 2012) for instances is more and more required since the cost of these experiments are also high.

2 Particle Transport Theory

Two types of particle transport methods are available in CFD simulations in general: the Eulerian and the Lagrangian method. The Eulerian method handles the particle phase as a

continuum and develops its conservation equations on a control volume basis, likewise for the fluid phase. The approximation of the Lagrangian method is different: it considers particles as a discrete phase and tracks the pathway of each individual particle (Zhang and Chen, 2007). The Lagrangian method is used mostly to predict the overall particle dispersion pattern and the temporal development of the mean concentration, and is base of further developments, like the viscoelastic particle model (Losurdo, 2009).

In the presently used software, in the ANSYS CFX, the particle transport modelling is a type of multiphase model, where particulates are tracked through the flow in a Lagrangian way, rather than being modelled as an extra Eulerian phase. The full particulate phase is modelled by just a sample of individual particles. The tracking is carried out by forming a set of ordinary differential equations in time for each particle, consisting of equations for position, velocity, temperature, and masses of species. These equations are then integrated using a simple integration method to calculate the behaviour of the particles as they traverse the flow domain (ANSYS, 2012).

Within the particle transport model, the total flow of the particle phase is modelled by tracking a small number of particles (solid particles and drops in the present case) through the continuum fluid. The application of Lagrangian tracking in CFX involves the integration of particle paths through the discretized domain. Individual particles are tracked from their injection point until they escape the domain or some integration limit criterion is met. Each particle is injected, in turn, to obtain an average of all particle tracks and to generate source terms to the fluid mass, momentum and energy equations. Because each particle is tracked from its injection point to final destination, the tracking procedure is applicable to steady state flow analysis (ANSYS, 2012).

The particle displacement is calculated using forward Euler integration of the particle velocity over time step, δt. As $dx_p/dt=Up$, the particle displacement is given as: (ANSYS, 2012):

$$x_p^n = x_p^0 + U_p^0 \delta t, \tag{1}$$

here the superscripts 0 and n refer to old and new values respectively, and U_p^0 is the initial particle velocity. In forward integration, the particle velocity calculated at the start of the time step is assumed to prevail over the entire step. At the end of the time step, the new particle velocity is calculated using the analytical solution to the particle momentum equation (ANSYS, 2012):

$$m_p \frac{dU_p^0}{dt} = F_{all} \tag{2}$$

F_{all} is the sum of all forces acting on a particle as drag force, buoyancy force due to gravity, forces due to domain rotation (centripetal and Coriolis forces), virtual (or added) mass force, and pressure gradient force.

The aerodynamic drag force on a particle is proportional to the slip velocity, U_s, between the particle velocity (U_p) and the fluid velocity (U_F) (ANSYS, 2012):

$$F_D = \frac{1}{2} C_D \rho_F A_F |U_S| U_S = \frac{1}{2} C_D \rho_F A_F |U_F - U_P| (U_F - U_P) \tag{3}$$

where C_D is the drag coefficient and A_F is the effective particle cross section. The drag coefficient; C_D, is introduced to account for experimental results on the viscous drag of a solid sphere. The particle momentum source due to drag is calculated from the following equation (ANSYS, 2012):

$$\frac{dS}{dt} = -F_D = -\frac{1}{2} C_D \rho_F A_F |U_S| U_S \tag{4}$$

The source term, S, added to the continuous phase is then multiplied with the number rate for that particle.

At low particle Reynolds numbers (the viscous regime), the drag coefficient for flow past spherical particles may be computed analytically. The result is Stokes' law: $C_D=24/Re$ (if Re <<1). For particle Reynolds numbers, such that are sufficiently large for inertial effects to dominate viscous effects (the inertial or Newton's regime), the drag coefficient becomes independent of Reynolds number: C_D=0.44 (if 1000<Re <1-2 x 10^5). In the transitional region between the viscous and inertial regimes, 0.1<Re<1000 for spherical particles, both viscous and inertial effects are important. Hence, the drag coefficient is a complex function of Reynolds number, which must be determined from experiment. This has been done in detail for spherical particles. Several empirical correlations are available. The one available in CFX is from Schiller and Naumann (1933) (ANSYS, 2012):

$$C_D = \frac{24}{Re}\left(1 + 0.15 Re^{0.687}\right) \tag{5}$$

CFX modifies this to ensure the correct limiting behaviour in the inertial regime by taking (ANSYS, 2012):

$$C_D = max\left(\frac{24}{Re}\left(1 + 0.15 Re^{0.687}\right), 0.44\right) \tag{6}$$

To model the behaviour of the different particles, besides the air as ideal gas, a particle transport solid/fluid is defined in the duct domain.

3 Contributors of Particle Tracking

The particle path computation is a complex problem. Besides the general CFD governing equations (which are not introduced here because they can be found in many textbooks), several further effects have to be taken into consideration. In case of particles traveling by the flow, the behaviour of the coupled system can be influenced by the material properties; the size and the shape of the particles; gravity, inertia and buoyancy forces; interaction effects between the particles, flow and the wall; and particle break up. The modelling approaches of the most relevant phenomena are introduced in the following subchapters.

3.1 Material Properties, Particle Definition

Since all materials have different properties, like molar mass, density, reference temperature, some materials have to be defined, like the ice. Usually CDF software doesn't contain the properties of ice particles; these have to be inserted manually, while other materials, like water, are already available. In the present case, it is necessary to simulate the path of an ice particle, hence the following properties are going to be used (Toolbox, 2016):

- 18.02 molar mass
- 0.917 g/cm^3 density
- -2 °C Reference temperature

The morphology or the phase of the particles can be defined by setting "particle transport fluid" or particle transport solid" model. In the former case the shape of the particle is determined by the aerodynamic forces and surface tension, while in the latter case the particle geometry has to be defined.

3.2 Particle Diameter Distribution

The particle diameter distribution is a significant contributor of the particles' behaviour, if they are not same-sized. A particle diameter distribution can optionally be set for a domain. If specified, then the distribution applies to all boundaries where particles are injected in that domain. The diameter distribution settings can be the following (ANSYS, 2012):

- Specified diameter: A constant specified particle diameter is set for all particles, and they are considered as spherical shaped, have a constant and uniform diameter, which value is defined.
- For non-uniform diameter distribution usually more settings are available, like if there are only the distributions of the particle diameter and standard deviation are given.

3.3 Particle Shape Factors

The non-spherical shaped particles' behaviour is significantly different, if drag or collision is considered. To handle these differences constant factors should be set, which modifies the drag force, mass and heat transfer correlations (ANSYS, 2012):

- A Cross Sectional Area Factor has to be included to modify the assumed spherical cross section area to allow for non-spherical particles. The factor is multiplied by the cross section area calculated assuming spherical particles. This affects the calculated drag force.
- The Surface Area Factor is for a non-spherical particle, the ratio of the surface area to the surface area of a spherical particle with the same equivalent diameter. This factor affects both mass transfer and heat transfer correlations.

3.4 Buoyancy Model

Natural and mixed convection flows and flows in which gravity is important can be modelled by the inclusion of buoyancy source terms. Natural convection refers to the case where convection of the fluid is driven only by local density variations. Mixed convection refers to the case where convection of the fluid is driven by both a pressure gradient and buoyancy forces. In multi-component flows, variations in the mass fraction cause density variations because each component usually has a different density. In multiphase flows, including particle transport modelling, the difference in density between the phases results in a buoyancy force. For ideal gases and real fluids, local pressure variations also cause changes in density. For calculations involving buoyancy, the gravity vector components in x, y and z must be set. These are interpreted in the coordinate frame for the domain.

In Ansys CFX there are two available Buoyancy models: (ANSYS, 2012)

- Full Buoyancy Model (Density Difference): For single phase flows, this model is used when the fluid density is a function of temperature or pressure (which includes all ideal gases and real fluids) and when a multi-component fluid is used. For Eulerian multiphase or particle tracking, it is also set even if all phases have constant density.
- Boussinesq Model: For many applications involving buoyancy, it is sufficient to assume a constant fluid density when the change in density over the expected range of conditions is relatively small. This is often true for many liquids. When the fluid density is not a function of pressure or temperature, the Boussinesq model is employed. The Boussinesq model is used by default for single-phase, single component simulations with heat transfer, using a constant density General Fluid.

3.5 Buoyancy in Multiphase Flow

As it was mentioned before difference in density between phases produces a buoyancy force in multiphase flows (including particle tracking). For this reason, buoyancy is almost always important in multiphase flows. For multiphase flows, it can be important to correctly set the buoyancy reference density. For a flow containing a continuous phase and a dilute dispersed phase, the buoyancy reference density to that of the continuous phase must be set. This is because the pressure gradient is nearly hydrostatic, so the reference density of the continuous phase cancels out buoyancy and pressure gradients in the momentum equation.

3.6 Buoyancy Turbulence

If fully buoyancy model or Boussinesq buoyancy model is applied, a buoyancy production term is included in the k (turbulent kinetic energy) equation and also in ε (dissipation rate) equation. This source term must be positive. Since in our investigation this option was not used, further details are not included in this paper.

3.7 Particle Rough Wall Model

The interaction between a particle and wall has complex physics, furthermore not all aspects are well understood. Influencing factors are the wall temperature, wall material and roughness, impact angle and impact velocity, the existence of a wall film and further parameters (ANSYS, 2012).

On a per-boundary or per-domain basis rough wall model can be set. The wall roughness model could be important if the roughness height has a same magnitude as the particle diameter and the sufficient information about the surface conditions are available (see Fig. 1). In this case the Sommerfeld-Frank rough wall model could be applied.

To account for the influence of wall roughness on the particle-wall collision, the irregular bouncing model of Frank is used. This model is based on the virtual wall model that was proposed by Sommerfeld. In this model (see Fig. 1), it is assumed that the reflection of a particle at a rough wall can be modelled as the reflection of the particle at a virtual wall that is inclined with an angle of "γ_w" relative to the real wall.

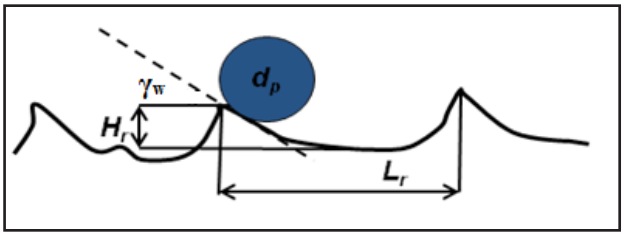

Fig. 1 Interaction of particle-wall at a rough wall (Frank, 2002)

This inclination angle "γ_w" is sampled from a Gaussian distribution with a mean value of 0° and a standard deviation of "$\Delta\gamma$". The standard deviation depends on the particle diameter and the roughness parameters as follows (Frank, 2002):

$$\Delta y = \begin{cases} \arctan\dfrac{2\Delta H_r}{L_r} \;\; if \;\; d_p < \dfrac{L_r}{\sin\left(\arctan\dfrac{2H_r}{L_r}\right)} \\ \arctan\dfrac{2H_r}{L_r} \;\; if \;\; d_p > \dfrac{L_r}{\sin\left(\arctan\dfrac{2H_r}{L_r}\right)} \end{cases} \tag{7}$$

Where the parameters should be defined when this model going to be used:

- L_r is the mean cycle of roughness (the average distance between peaks of wall material)
- H_r is the mean roughness height (R_z is given the same basically)
- ΔH_r is the standard deviation of the roughness height (depends on the surface finish method and tool parameters)

3.8 Particle Fluid Pair Coupling Options

Particles can be either fully coupled to the continuous fluid or can be one-way coupled. Fully coupled particles exchange momentum with the continuous phase, allowing the continuous flow to affect the particles, and the particles to affect the continuous flow. Full coupling is needed to predict the effect of the particles on the continuous phase flow field but has a higher CPU cost than one-way coupling. One-way coupling simply predicts the particle paths as a post-process based on the flow field and therefore it does not influence the continuous phase flow field.

3.9 Surface Tension Coefficient

This should be set in either of the following two cases (ANSYS, 2012):

- For a Continuous Fluid / Dispersed Fluid pair when wanted to be modelled the Drag Force using either the Grace or Ishii Zuber models. The flow must also be Buoyant to allow these models to be selected.
- When the surface tension model is used. (In case of Flows with free surfaces modelling.)

During simulating the behaviour of different sized water droplets it is essential to determine the surface tension coefficient.

3.10 Momentum Transfer - Drag Force

For a particle of simple shape, immersed in a Newtonian fluid and which is not rotating relative to the surrounding free stream, the drag coefficient, C_D, depends only on the particle Reynolds number. The function $C_D(Re)$ may be determined experimentally, and is known as the drag curve. Different models are available for the drag curve, and the drag coefficients can be specified directly. The following drag models are available (ANSYS, 2012):

- Schiller-Naumann model *(for solid/fluid particles)*: This should only be used for solid spherical particles, or for fluid particles that are sufficiently small that they may be considered spherical. For non-spherical particles, you should supply the drag curve from experiment. As the Schiller Naumann correlation is derived for flow past a single spherical particle, it is only valid in the dilute limit of very small solid phase volume fractions.
- Wen Yu model *(for solid particles)*: The Wen Yu correlation is valid for solid phase volume fractions at least up to 0.2, and probably higher.
- Gidaspow model *(for solid particles)*: For very dense gas-solid or liquid-solid flows, such as occur in fluidized bed applications recommended.
- Ishii-Zuber model *(for fluid particles)*: This is applicable to general fluid particles (drops and bubbles), for any pair of phases.
- Grace model *(for solid particles)*: This model was developed using air-water data and produces better results for air-water systems.

Both the Ishii-Zuber and Grace Drag Models make explicit use of the gravity vector and surface tension coefficient. Hence, both are only available for buoyant multiphase flows when a surface tension coefficient has been specified. The fluid morphologies must be Continuous and Dispersed Fluid respectively (ANSYS, 2012).

3.11 Non-drag Forces Acting on the Particles

There are many forces can be considered, which are non-drag forces. Basically it depends on the density ratio of the continuous fluid and the dispersed fluid (ANSYS, 2012):

- Lift force: The lift force is proportional to the continuous phase density. Hence, it is mainly significant when the dispersed phase density is either less than, or of the same order of magnitude as the continuous phase density. Also, it is proportional to the continuous phase shear rate. Hence, it is most significant in shear layers whose width is comparable to the dispersed phase mean diameter.
- Virtual mass force: The virtual mass force is proportional to the continuous phase density, hence, is most significant when the dispersed phase density is less than the continuous phase density. Also, by its nature, it is only significant in the presence of large accelerations, for example, in transient flows, and in flows through narrow restrictions.
- Turbulent Dispersion Force: Turbulent dispersion forces result in additional dispersion of particles from high volume fraction regions to low volume fraction regions due to turbulent fluctuations. The Particle Dispersion model is available to account for the turbulent dispersion force. This force is only important for small particles (approximately smaller than 100 microns for water drops in air) and when one wants to see the dispersion. For example, even when the particle tracks are affected by turbulence, the effect of the particles on the continuous phase is usually the important process, and this is not affected by the turbulence. The turbulent dispersion force is only active in regions where the turbulent viscosity ratio is above the value specified by "Eddy Viscosity Ratio Limit". The default value is 5. Turbulent dispersion can only be used if a drag force is specified. Therefore, it is not possible to combine turbulent dispersion with a user-specified momentum source term for the drag.
- Pressure gradient force: The pressure gradient force results from the local fluid pressure gradient around the particle. This force is only important if large fluids pressure gradients exist and if the particle density is smaller than or similar to the fluid density.

3.12 Particle Breakup Model

The particle breakup models allow you to simulate the breakup of droplets due to external aerodynamic forces. But during droplet breakup, the particle shape may be distorted significantly and it might be desirable to modify the drag law to account for the influence of the particle distortion. There must be distinguished Primary and Secondary breakup (ANSYS, 2012):

- Primary breakup model support will only be available for particle injection regions and not for boundary condition, and on particle injection regions, primary breakup will only be available for cone type injection, and only if the nozzle cross-sectional area is larger than zero.
- Secondary breakup model describes the breakup of a liquid jet into droplets that is caused by a combination of different mechanisms: turbulence within the liquid phase, implosion of cavitation bubbles and external aerodynamic forces acting on the liquid jet. Depending on the injection parameters such as the relative velocity between liquid and gas, the liquid and gas densities and the liquid viscosity and surface tension the contribution of each of the above mechanisms to the spray breakup varies. Breakup regimes are typically classified in terms of the dimensionless numbers: Weber Number (We) and Ohnesorge number (Oh), as given by:

$$We = \frac{\rho_F V_{slip}^2 d_P}{\sigma} \tag{8}$$

$$Oh = \frac{\mu}{\sqrt{\rho_P \sigma d_P}} \tag{9}$$

Here the Weber number contains the slip velocity (relative velocity of the particle related to the fluid as mentioned above) and the subscript "*P*" refers to the droplet (particle) and the subscript "*F*" refers to the surrounding fluid. If a droplet is exposed to a gas flow, significant deformation starts at a Weber number of unity. Above a certain value of the Weber number, the droplet deformation leads to breakup. The Weber number values for the breakup regimes boundary vary based on the applied theory but typically no breakup occurs if the Weber number is below 12.

Reitz and Diwakar Breakup Model distinguishes between two breakup regimes: bag breakup and stripping breakup only. Breakup occurs if Weber number is above the "critical" (here the critical Weber number is defined constant value as 6).

In the **Schmehl Breakup Model** the droplet deformation and breakup times are based on experimental findings. The defined characteristic time (t^*) could be computed based on the flow (density), the particle (diameter and density) and the slip velocity. The time to deform a particle from a sphere into a disk shape and this time is approximately constant (ANSYS, 2012):

$$t_i = 1.6 \cdot t^* \tag{10}$$

The second phase of breakup, which is characterized by further distortion of the droplet to its final destruction based on the

local Weber number itself where $c(Wb)$ is a constant depend on the local Weber number (ANSYS, 2012):

$$t_{br} = c\left(Wb\right) \cdot t^{*} \tag{11}$$

Breakup could occur if the Weber number exceeds the critical Weber number (ANSYS, 2012):

$$Wb_{crit} = 12 \cdot \left(1 + 1.077 \cdot Oh^{1.6}\right) \tag{12}$$

There are three breakup regimes if the Weber number is over the critical value: Bag, Multimode and Shear breakup regimes. A random breakup time computed between the "t_i" and "t_{br}" resulted time values (based on which breakup regime is present) and if the particle lifetime (while the particle is tracked, so from the inlet to the outlet) is exceed the computed breakup time above, than breakup occurs and the "children" droplets diameter and velocity computed. This model could also consider the modified drag on the distorted drop (importance mentioned above), this option is "Schmehl Dynamic Drag Model" that computes the drag coefficient based on the local Reynolds number (by a 3rd order equation). While many particle drag models assume that the droplet remains spherical throughout the domain, this is not always the case and the particle shape may be distorted significantly. In the extreme case, the particle shape will approach that of a disk. The drag coefficient is highly dependent on the particle shape and it is therefore desirable to modify the standard drag laws to account for the effects of droplet distortion.

O'Rourke and Amsden proposed the so-called **Taylor Analogy Breakup (TAB) Model** that is based on the Taylor analogy. Within the Taylor analogy, it is assumed that the droplet distortion can be described as a one-dimensional, forced, damped, harmonic oscillation similar to the one of a spring-mass system. This model assuming that the droplet viscosity acts as a damping force and the surface tension as a restoring force during oscillation. Breakup only occurs if the particle distortion exceeds unity, which means that the deviation of the particle equator has become larger than half the droplet radius. There are many model constants to define by applying this method, for further details see the reference ANSYS, 2012. This model could also consider the modified drag on the distorted drop by "Liu Drag Model". It is a linear interpolation between the spherical and disk geometries for drag coefficients.

There are two further models (improvements of TAB model) called ETAB and CAB. ETAB (the Enhanced TAB model) uses the same droplet deformation mechanism as the standard TAB model, but uses a different relation for the description of the breakup process. It is assumed that the rate of child droplet generation is proportional to the number of child droplets, because it has been observed that the TAB model often predicts a ratio of child to parent droplet is too small. This is mainly caused by deformation parameters initial values. The CAB (Cascade Atomization and Breakup Model) contains further improvement on the ETAB in child droplet size computation. For all of the further models (ETAB and CAB) "Liu Drag Model" could be applied just like in case of the original TAB method (ANSYS, 2012).

3.13 Particle Collision

In classical Euler-Lagrange modelling, collisions between particles are not possible because the presence of other particles is not accounted for. The stochastic particle-particle collision model (by Oesterlé and Petitjean, which has been extended by Frank, Hussmann et Al, and Sommerfeld) takes interparticle collisions into consideration while the trajectories are still calculated sequentially. The main advantage of the model is the possibility of sequential trajectory calculation by creating virtual collision partners sampled from local statistical values. This offers a high potential of parallelization and therefore facilitates – in conjunction with the highly parallelized Solver for the gas-phase – its use in industrial applications as a major advancement in the simulation of dense gas-particle flows. The model extension by Sommerfeld additionally takes into account a possible correlation between the velocity fluctuations of adjacent particles. The following steps summarize the implementation of this model (ANSYS, 2012):

- Calculate the instantaneous velocity of the virtual collision partner.
- Determine the collision probability and decide whether or not a collision occurs.
- *If collision occurs:*
  - Compute position of virtual collision partner.
  - Calculate binary collision and adjust particle velocities.
- *If collision does not occur:*
  - Particle velocities remain unchanged in the event of no collision.
- Discard the virtual particle.
- Update average particle quantities and local statistical moments in each control volume.

The requirements for the applicability of particle-particle collision model are outlined below:

- High mass loading
- Moderate volumetric concentration (<~ 20%)
- The model is limited to binary collisions only and follows the following criteria:
  - Inter-particle distance is much greater than the particle diameter
  - Aerodynamic forces dominate
  - Not suitable for fluidized beds
  - $\rho_{particle} \gg \rho_{fluid}$
- Spherical particles

3.14 Coefficient of Restitution (Particle-Particle)

There are two types of COR (coefficient of restitution) should be distinguished. The COR for the particle-particle collisions have to be defined, at this section. This coefficient

of restitution is a measure of the amount of bounce between two objects. Specifically, it is the ratio of the velocities of the objects before and after an impact, and can be described mathematically as (ANSYS, 2012):

$$C = \frac{V_{2f} - V_{1f}}{V_{2i} - V_{1i}} \tag{13}$$

- V_1 is the velocity of the first object
- V_2 is the velocity of the second object
- i and f subscripts indicate initial and final velocity, respectively.

Since the investigation between two droplets is a really hard – or almost impossible to carry out, the initial of the assumption are some literature which estimated the COR during droplets collide with a surface (Abedi, 2009).

These studies are about the heat transfer conditions regarding the cooling conditions in case of a liquid stream reaches a heated surface. One of the studies contains a summary of the others and estimate an equation for the COR as a function of the Weber-number for heated surfaces above the Leidenfrost point (Issa, 2004). Behind this point just before the collision because of high temperature (heat convection and radiation near the wall) a thin gas layer could be formed on the surface of the droplet and the collision become more elastic, so the COR could increase significantly.

Other study investigates a particle separator for sand particles but these results could not be applied in our investigation because of the properties and water properties are different (Issa, 2004). In another study super-hydrophobic surfaces were investigated as originally new technology (van der Wal, 2006), but because of dramatically increased contact-angle of a drop on a surface, the measured COR values are much higher than in our test cases required.

3.15 Static and Kinematic Friction Coefficients

The friction of coefficients should be defined between the particles if collision occurs, that has an influence on the particles velocity components after the collision. Friction coefficients in static and kinetic conditions must be distinguished. For water droplets these values should be set zero because of elastic collision estimated and the drops could deform despite of sliding on each other, and this phenomenon is considered by the applied particle breakup model.

3.16 Particle-Wall interaction

The particle-wall interaction has to be set for the "Wall" boundary conditions separately from the main fluid domain boundary conditions. There are two main approaches are distinguished a "Equation Dependent option" and "Wall film option".

In an "Equation Dependent option" the droplet is reflected off a wall and the momentum change across the collision is described using the perpendicular and parallel coefficients of restitution (COR). These values have the same meanings as it was described earlier. There could be a "Minimum impact angle" set also to specify the minimum impact angle. Below this impact angle, particles will be stopped and sliding along the wall. But note that setting the perpendicular coefficient of restitution to a small positive number is not a valid way to simulate particle sliding along a wall. Currently there is no method for accurately simulating this type of particle sliding (ANSYS, 2012).

There are two models can be selected for the particle-wall interaction in case of considering a wall film (layer) build-up along the wall (ANSYS, 2012):

- The Elsaesser Particle-Wall interaction model: This model distinguishes three regimes as cold wall with wall film, and hot wall with and without wall film. Based on these regimes, material of the wall (have to be selected) and its roughness, local temperature and Weber number values the particle behaviour upon the impact could be estimated precisely. The main problem with the Elsaesser particle-wall interaction model is mainly targeted towards the application in internal combustion engines, because most of the correlations used in the model are strictly only valid for gasoline type of fuels and assume that the wall material is aluminium. The model uses over 50 different model constants internally.
- Stick-to-wall model: The model enforces all particles that hit a wall to become part of the wall film, regardless of their impact velocity or impact angle. Also, particles that are collected on a wall are able to interact with their surroundings by exchanging mass and energy (for example, during the droplet evaporation).

4 Presentation of the Simulation Cases

Recent study aims to investigate the particle separation efficiency of an air intake device of a small aircraft. 2 CFD simulation cases have been carried out to the same geometry, but applying different particles, as 2.66 mm liquid water droplets and 16 mm hailstones.

4.1 Geometry and the created mesh

The power plant to be considered in the ESPOSA project is a small gas turbine designed for the airplane, which is a high-wing, turboprop, multi-purpose aircraft for transportation passengers and/or cargo. The nose landing gear of the airplane is retractable; the tail unit is T-shaped. Up to 9 passengers can be carried in the unpressurized cabin with two cabin crew members. Type AVIA tractor propellers are installed on the engines.

The gas turbine contains a static inlet guide vanes. These deflect the airflow to the compressors, and upstream of that the particle separator, de-icing unit is located. This component is responsible to remove the rain, ice particles, or dust from the airflow. The duct intake, the de-icing device and the inlet guide

vane together represents the air intake unit, which is the subject of an improvement process in order to increase the particle separation efficiency, and to minimize the pressure drop upstream of the compressor. The CAD model of the improved assembly has been provided by VZLU Aerospace Research & Test Establishment.

In order to make the simulation's efficiency higher, the air intake unit has been separated into 3 domains: the intake duct, the centre part with the de-icing unit and inlet guide vanes, and an extracted volume at the compressor inlet surface, which makes possible to leave the boundary condition undisturbed. In the inlet surface this extraction could be neglected since the inlet boundary conditions have been resulted from a complex, previously completed simulation, and furthermore, the duct intake domain is enough to eliminate the disturbances. This separation was necessary, because the first and third component are simple compared to the centre unit, so these two have been discretized with hexagonal mesh elements, while the centre unit with using tetra elements.

The hybrid mesh makes possible to reduce the computation time demands, meanwhile to improve the accuracy of the results. The full mesh has been built up from 13,294,772 elements and 6,203,530 nodes. The elements are distributed between the 3 domains according to Table 1. 15 inflation layers have been used on the walls and the centroid of the first cell from the solid surface has been determined to keep the y+ values below 300, according to the requirements of the applied Shear Stress Transport turbulence model with wall function.

Table 1 The element and node number of the 3 applied domains

	Duct intake	Centre unit	Engine intake
Element number	1,090,073	9,785,463	2,419,236
Node number	1,056,000	2,787,530	2,360,000

The geometry and the final mesh is illustrated in Fig. 2 and Fig. 3.

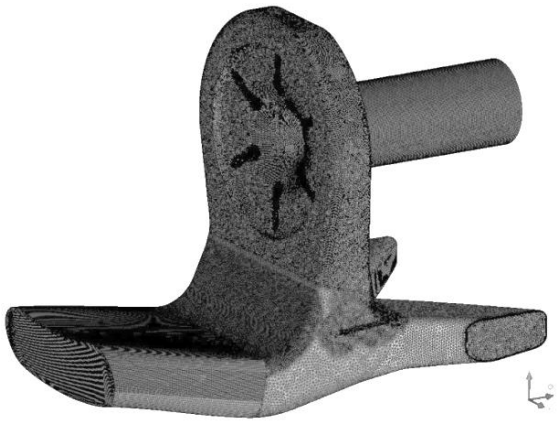

Fig. 2 The geometry of the air intake, and the built-up mesh

Fig. 3 The symmetry cross-section of the intake channel (without extracted volume), representing the inflation layers

4.2 Physical Conditions and Settings

The modelling approaches, material properties and boundary conditions were set for each case separately. These characteristics are the fluid parameters in general, the inflow and outflow specifications and particle behaviour for different materials. The flow domains were set to air as an ideal gas. The reference pressure of the domains has been calculated from the cruise altitude of the aircraft (3048 m) based on the International Standard Atmosphere parameters, resulted in 69,682 Pa. The buoyancy model was responsible to simulate the effect of the gravity field, since the behaviour of the particles is strongly affected. In all of the test cases the Full Buoyancy Model (Density Difference) was applied because it is recommended for particle tracking even if all phases have constant density, moreover here the airflow density could vary depends on the temperature and pressure. As buoyance reference density the airflow's (approx.) density was set as 1 [kg/m^3] in any cases.

Although it has negligible influences, since no heat transfer has been included in the simulation, total energy model has been applied, which includes the viscous work term. As it was mentioned already, the steady state model's turbulence has been handled by using Shear Stress Transport (SST) turbulence model, and 5 % inlet turbulence intensity has been set in the inlet surface originated from the result of a former, complex simulation.

A complex, previously completed simulation provided the necessary boundary conditions, summarized in Table 2. Ambient air section, propeller, nacelle with engine intake duct and wing were included in that simulation.

Particle mass flow rate and injected particle number should be computed and defined as a boundary condition. According to the engine icing requirements, the "density of the particles" (*g particle/m^3* air) was specified by the vehicle manufacturer (see Table 3). The effect of the two highest-sized contributions as water droplets: 2.66 mm and hailstones: 16 mm has been investigated for separation efficiency point of view in the present report.

Table 2 Parameters provided by the pre-simulation for particle number and separation calculation

Inlet	Outlet (engine intake)	Interface (ice remover outlet)
total pressure (relative): 6284.48 Pa	pressure (relative): -10519.9 Pa	pressure (relative): -2139.85 Pa
static pressure (relative): 2579.08 Pa	temperature: 267.644 K	temperature: 267.644 K
mass flow: 3.42523 kg/s	$V_{average}$: 164.534 m/s	density: 0.878686 kg/m^3
$V_{average}$: 88.3825 m/s	U: 160.182 m/s	mass flow: 1.48529 kg/s
U: 87.35 m/s, V: -12.94 m/s, W: -2.85 m/s	V: 8.78613 m/s	
density: 0.9255 kg/m^3	W: -5.41599 m/s	
temperature: 271.96 K, Mach: 0.267	density: 0.78648 kg/m^3	

Table 3 Requirements for particle number calculation

Particle type and size	Particle content (PC_{mass}) (g particle/m^3)
Water droplet: 20 μm	1 g/m^3
Water droplet: 2.66 mm	20 g/m^3
Ice crystal: 1 mm	5 g/m^3
Hailstone: 16 mm	7 g/m^3

At first, the volume flow rate of the air was determined based on the mass flow rate and averaged density values at the intake (the boundary conditions are coming from the previous simulation results introduced above):

$$\dot{V}_{air} = \frac{\dot{m}_{air}\left[\frac{kg}{s}\right]}{\rho_{air}\left[\frac{kg}{m^3}\right]} = \frac{3.43}{0.93} = 3.701\left[\frac{m^3}{s}\right] \tag{14}$$

A single particle mass could be computed weather it is considered as spherical:

$$m_{particle}\left[\frac{g}{particle}\right] = \frac{4\cdot\pi\cdot R^3_{particle}}{3}\cdot\rho_{particle} \tag{15}$$

According to the results the particle content can be estimated as [particle/m^3] by (16).

$$PC_{volume}\left[\frac{particle}{m^3}\right] = PC_{mass}\left[\frac{g}{m^3}\right] / m_{particle}\left[\frac{g}{particle}\right] \tag{16}$$

The number of particles injected within a second and the particles mass flow rate is calculated by the computed volume flow rate of air; V_{air}, PC_{volume} and $m_{particle}$ according to Table 4. The velocity and the direction of the incoming particles corresponded to the inlet flow velocity.

To model the behaviour of the different particles, besides the air as ideal gas, a particle transport solid/fluid is defined in the duct domain. For the water particles, the already defined water material is used, but for solid ice particles a new material has been created with the following properties: pure substance material in solid phase with 18.02 g/mol molar mass; 0.917 g/cm^3 density and -2° C reference temperature; thermodynamic state: solid.

In the simulation, the following settings have applied:

- Fully coupled option was applied in both test cases, because it was important to consider the two-directional interaction between the fluid and the particles.
- The inserted particles were considered as uniform and spherical shaped with the specified diameter values.
- Regarding the particle breakup of water droplets, the surface tension coefficient is required to compute the surface energy of the particle. So in case of water droplets investigated the surface tension coefficient is set to 0.0756 N/m^2 according to the surface tension coefficient of the water at 0 °C (Engineering Toolbox, 2016).
- In all test cases Schiller-Naumann drag model was applied, because all of the particles are considered as spherical.
- Concerning the non-drag type forces, Turbulent Dispersion Force option was not activated, because it is recommended to apply if the particle diameter is below 100 μm. Other types of non-drag forces acting on the particles were not applied also, because the particle density was higher than the continuous (fluid) phase has.
- Rough wall model was not used because the surface roughness of a hot rolled aluminium sheet metal is approximately 1-2 μm. The smallest particle (water droplet)

Table 4 Calculated particle weights, particle numbers in unit volume, injected particle numbers per second and particle mass flow rates

Particle type and size	$m_{particle}$ (g/particle)	PC_{volume} (particle/m^3)	Calculated particle numbers (particle/sec)	Applied/Injected particles (particle/sec)	Particle mass flow rate (kg/s)
Water droplet: 2.66 mm	9.855*10^{-3}	2029.48	7511.15	7511	7.402*10^{-2}
Hailstone: 16 mm	1.967	3.56	13.17	13	2.591*10^{-2}

is the 2.66 mm, and it has even around 1300 times greater diameter than the surface roughness of the intake channel.

- The stochastic particle-particle collision model takes interparticle collisions into consideration while the trajectories are still calculated sequentially. The main advantage of the model is the possibility of sequential trajectory calculation by creating virtual collision partners sampled from local statistical values. This offers a high potential of parallelization and therefore facilitates – in conjunction with the highly parallelized CFX-Solver for the gas-phase – its use in industrial applications as a major advancement in the simulation of dense gas-particle flows. According to the description above, Sommerfeld collision model is used in all test cases.
- The Coefficient of Restitution (COR) (particle-particle) was set to 1 (elastic collision) in case of 16 *mm* hailstones (solid phases), while in case of 2.66 *μm* water drops it was decreased to 0.1 because the probability of inelastic collision (limited surface energy, much more deformable).
- The parallel COR (particle-wall) was set to 1 in case of ice particles considering there was no energy loss in direction parallel to the wall, this velocity component remains constant. This represents elastic collision for the solid particles. Otherwise, in case of water investigated, perpendicular COR (particle-wall) was set to 0 in case of 2.66 *mm* water droplets to model the particle stick to the wall.
- The applicable friction coefficient ranges (Static – Dynamic) for the ice-ice particle interaction are found in Table 5 (Hypertextbook, 2016).
  Static friction coefficients as 0.1 and kinetic as 0.03 were applied between ice-ice particles.

Table 5 Static and kinematic friction coefficients between ice particles

Material pair	Static (μ)	Kinetic (μ)
Ice-ice	0.05-0.5	0.02-0.09

The location of the boundary conditions is shown in Fig. 4 and the corresponding physical values are extracted from Table 2.

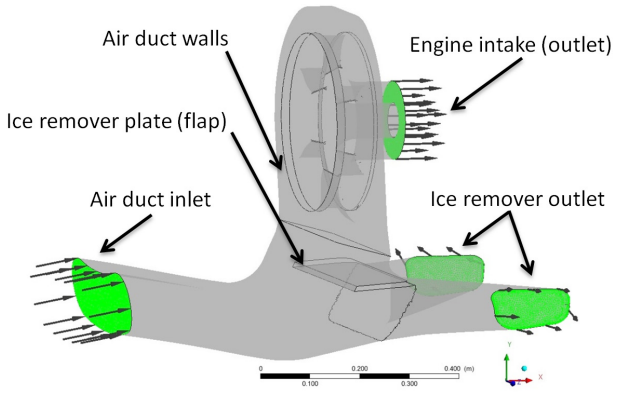

Fig. 4 Boundary conditions of the model

High resolution advection scheme has been used, similarly like in the case of the turbulence numeric option. Auto timescale has been applied, and the residuum target for RMS values was 10^{-6}.

In order to reduce the computation time demand, initially a simulation case has been carried out without any particles. The converged results have been applied in each further simulation case as initial conditions, so the iteration process could be minimized. 1000 additional iteration steps have been set in each simulation case.

5 Evaluation of Results

The base simulation without particles has executed for 1425 iteration steps, meanwhile the momentum residuum have converged below $2*10^{-4}$, the mass residuum has reached below $4*10^{-5}$. Each particle tracking simulation has run for 1000 more iteration steps. The simulation itself can be stated as converged, since all of the imbalances have converged below 1 % (see Fig. 5).

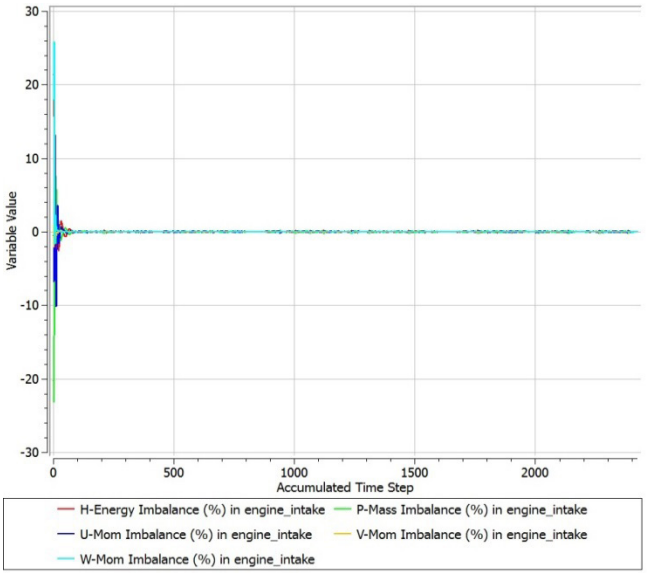

Fig. 5 The imbalances of the simulations

The base simulation required $3.873*10^5$ CPU wall clock seconds, and each particle tracking case added it with $1.659*10^5$ CPU wall clock seconds in average. On an average personal computer with 16 GB of RAM, and with an 8 core processor that means approximately 4+2 days.

5.1 Mesh Quality by y+

The numerical mesh has been created in line with the meshing guideline with especial care for the determination of the first cell thickness from the wall, the boundary layer thickness, the expansion ratio of the cell thicknesses and cell sizes. The *y*+ distributions are found in Fig. 6. The desired value of *y*+ is either ≈1 (less than or equal 2 to take the full advantage of the low-Reynolds formulation) or between 30 and 300 (in the

present case). Here, the *y*+ values are below 32. The quality of the mesh could be improved of course, but the actual configuration is considered as an acceptable balance between the accuracy and computational cost.

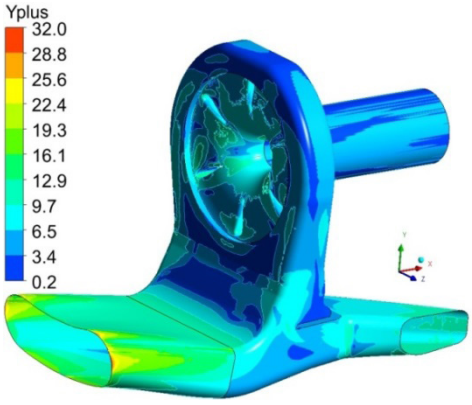

Fig. 6 The *y*+ distribution on the solid walls

5.2 General Flow Conditions

Since there are 2 different simulations, in the following only the most relevant results are presented. Inside the air intake channel the air flow slightly accelerates in the intake channel, than at the bend it separates, one part leaves the intake channel through the de-icing device outlet, the rest is directed through the inlet guide vanes to the engine's compressor inlet. The critical point of the system – from the viewpoint of the air flow's velocity is the outlet section of the inlet guide vanes, where the highest airspeed (249 m/s) is achieved due to the convex curvature effect. As the streamlines show in Fig. 7 the air flow for the most part is uniform, separations can be observed above the ice separator flap, and adjacent to the inlet guide vanes.

The absolute pressure distribution – see Fig. 8 – indicates the pressure drop of the duct (which should be minimized in parallel to the particle separation efficiency). In the engine intake cross-section the mass flow-averaged absolute total pressure was 71,817.62 Pa compared to the inlet total pressure, which was 75,966.48 Pa. This means 4148.86 Pa pressure drop and this 5.46 % relative difference is caused by the air intake device.

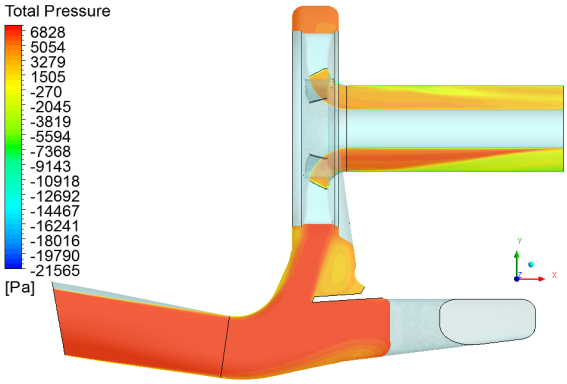

Fig. 8 Relative total pressure distribution in the mid symmetry cross-section of the air intake

This high pressure drop is justified since the de-icing mode of the construction is used only in the specific flight condition, and is not optimized for the engine air supply. In this case the most important factor is to prevent smaller-larger particles to get into the compressor rotor stage, because they can cause significant damages to the compressor and turbine blades, or in the case of heavy raining if water droplets get into the combustion chamber of the gas turbine, they can cause flame-out.

5.3 Particle Separation

According to the engine icing requirements, the effect of the two highest-sized particle as water droplet 2.66 mm and hailstone 16 mm has been investigated for separation efficiency point of view in the present subchapter.

In the case of the liquid particles the big water droplets move together with the air stream till the enter of the separator unit. The particle size and weight is high, which means that the particles have high inertia force to be separated and removed from the intake duct. Additionally, as soon as a water particle collides to the air intake wall, it splashes and basically stays on the wall. It can be concluded, that the particles will not move together with the airflow after the bending of the channel and so cannot enter into the engine. The trajectories are shown in Fig. 9. The separation efficiency is 100 % (see Table 6).

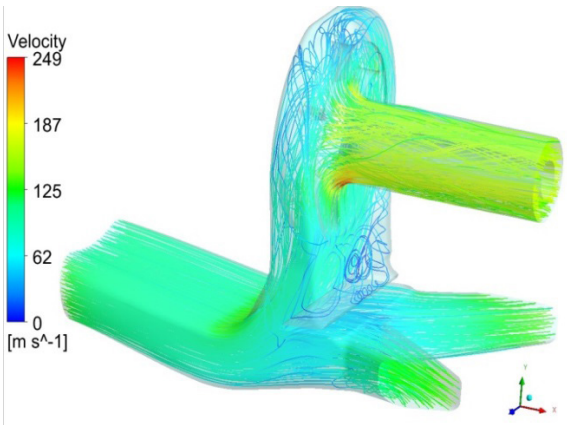

Fig. 7 Streamlines inside the air intake duct

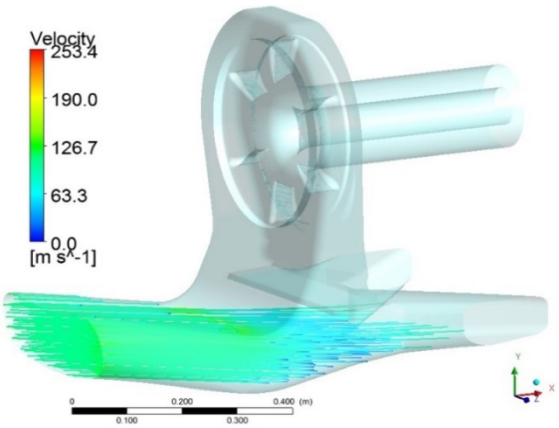

Fig. 9 Particle paths of the 2.66 mm rain droplets in the air intake device.

Table 6 Particle mass flow rates in the simulation cases in the inlet and outlet surfaces, and the calculated separation efficiency

Particle mass flow rates: $\left[\frac{kg}{s}\right]$	m_{inlet}	$m_{separated}$	m_{engine_inlet}	Separation efficiency
Water droplet: 2.66 mm	0.07402	0.07402	0	100 %
Hailstone: 16 mm	0.0025415	0.0025415	0	100 %

In the case of the 16 mm hailstones, the big ice particles move together with the air stream till the enter of the separator unit or till their first collision with the wall. The particle size and weight is high in this case also, which means that the particles have high inertia force to be separated and removed from the intake duct. Moreover, the solid particles are not breaking up during colliding with the walls, they rebound elastically, and their erosion has been neglected. According to that, a bouncing path is created, which cause also that the particles cannot reach the compressor intake surface as it is shown in Fig. 10. The separation efficiency was also 100 % in this case also (see Table 6).

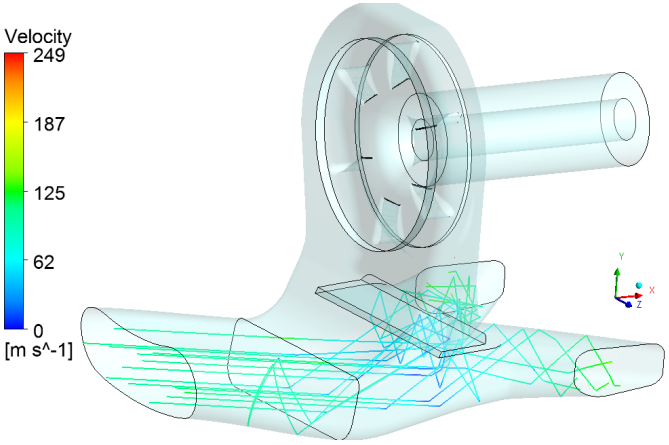

Fig. 10 Particle paths of the 16 mm hailstones in the air intake device.

According to the presented results it can be summarized that the engine intake ice removal device has high separation efficiency for both water droplets 2.66 mm and hailstones 16 mm. However, further analyses are necessary for different particle sizes and materials given in the design specification, and at other operational conditions to determine the separation efficiency at these modes also.

Structural and explicit dynamic analyses were not completed in the present project. Hence, further investigations could be done to simulate the effect of large hailstone impacts on the air intake duct, since the significantly large weight can cause damages to the intake duct structure.

6 Summary

Present paper introduces detailed description of a RANS and Lagrangian method based CFD simulations created for particle tracking in order to provide an accurate and effective way for for aerodynamic design and analyses. The investigated geometry was the air flow of a small aircraft engine air intake channel and its ice and particle separator device. A hybrid mesh was built up to perform the 2 simulation cases, determined by the design specification for the investigated particles. The effect of the water droplet 2.66 mm and hailstone 16 mm was analysed for separation efficiency point of view. The simulations' results have confirmed the expectations about the general behaviour of the particles, and it can be concluded that the investigated geometry is 100 % efficient to separate out the particles under investigation from the engine intake channel.

Acknowledgement

The work has been performed within the ESPOSA project (Grant Agreement No. ACP1-GA-2011-284859-ESPOSA) funded by the 4th call of the FP7 Cooperation Work Programme. The investigation also supports other applications, so the developed method is intended to apply in " Small aircraft hybrid propulsion system development" supported by Hungarian national EFOP-3.6.1-16-2016-00014 project titled " Investigation and development of the disruptive technologies for e-mobility and their integration into the engineering education".

References

Abedi, M. (2009). *Effect of restitution coefficient on inertial particle separator's efficiency.* M.Sc. Thesis, Northeastern University, Boston, USA.

Anandharamakrishnan, C. (2013). *Computational Fluid Dynamics Applications in Food Processing*. Springer-Verlag, New York. https://doi.org/10.1007/978-1-4614-7990-1

ANSYS. (2012). ANSYS CFX-Solver Theory Guide. USA: ANSYS, Inc. Southpointe, 275 Technology Derive Canonsburg, PA 15317.

Beneda, K. (2008). Dynamic Nonlinear Mathematical Model of Active Compressor Surge Control Devices. In: 11th Mini Conference On Vehicle System Dynamics, Identification and Anomalies, 2010. pp. 583-591.

Bojdo, N., Filippone, A. (2011). Helicopter Engine Intake Barrier Filter Design. Paper presented at the European Rotorcraft Forum, At. Milan, Italy.

Brun, K., Kurz, R., Nored, M. (2012). Analysis Of Solid Particle Surface Impact Behavior In Turbomachines To Assess Blade Erosion And Fouling. Paper presented at the Proceedings of the Forty-First Turbomachinery Symposium, Houston, Texas.

Chang, Y., Adamsen, T. C. H., Pisarev, G. I., Hoffmann, A. C. (2013). PEPT: An invaluable tool for 3-D particle tracking and CFD simulation verification in hydrocyclone studies. Paper presented at the EPJ Web of Conferences 50, 05001.

Engineering Toolbox. (2016). Surface Tension of Water in Contact with Air. [Online]. Available from: http://www.engineeringtoolbox.com/water-surface-tension-d_597.html [Accessed: 15th October 2016]

Frank, T. (2002). Parallele Algorithmen für die numerische Simulation dreidimensionaler, disperser Mehrphasenströmungen und deren Anwendung in der Verfahrenstechnik. PhD Thesis, Shaker Verlag GmbH. (in German)

Hanzal, V. (2015). Aerodynamic optimization of the engine nacelle shape, Czech Aerospace Proceedings, 2015(2).

Hargitai, Cs. (2012). Effect of parameters of inland vessel semi empirical motion equations on transient motion phenomena. In. Proceedings of the TVL: Second Scientific Workshop on Transport, Vehicle and Logistics organized by the PhD Schools of the Faculty of Transportation Engineering and Vehicle Engineering, 2012. pp. 1-6.

Hellmann, A., Schmidt, K., Pitz, M., Ripperger, S. (2014). Comparison of measurement and simulation of particle deposition at charged microfibers. Paper presented at the Aerosol Technology, Karlsruhe.

Hypertextbook, T. P. (2016). Friction – Discussion. [Online]. Available from http://physics.info/friction/ [Accessed: 18th May 2016]

Issa, R. J. (2004). Numerical Modeling Of The Dynamics And Heat Transfer Of Impacting Sprays For A Wide Range Of Pressures. PhD Thesis, University of Pittsburgh, Pittsburgh.

Lindberg, S. (2015). Numerical simulation of particle soiling in the engine compartment of a bus. M.Sc. Thesis, Chalmers University Of Technology, Göteborg, Sweden.

Losurdo, M. (2009). Particle Tracking and Deposition from CFD Simulations using a Viscoelastic Particle Model. Ph.D Thesis, University of Rome, Rome, Italy.

Meijering, E., Dzyubachyk, O., Smal, I. (2012). *Methods for Cell and Particle Tracking.* Imaging and Spectroscopic Analysis of Living Cells, 504 of Methods in Enzymology, 183-200.

Musgrove, G. O., Barringer, M. D., Thole, K. A., Grover, E., Barker, J. (2009). Computational design of a louver particle separator for gas turbine engines. Paper presented at the Proceedings of ASME Turbo Expo 2009: Power for Land, Sea and Airv.

Rohács, D. (2015). The current state and vision of the national transport safety: Air transportation. In: Horváth, Zs. Cs., Kisgyörgy, L., Ágoston, Gy., Rohács, D. (eds.) *Actual questions of transport safety in the new millennium*. (pp. 64-88.), Universitas-Győr Nonprofit Kft., Győr.

Toolbox, E. (2016). *Thermal properties of ice.* [Online]. Available from: http://www.engineeringtoolbox.com/ice-thermal-properties-d_576.html [Accessed: 15th May 2016]

van der Wal, B. P. (2006). *Static and Dynamic Wetting of Porous Teflon® Surfaces.*

Zhang, Z., Chen, Q. (2007). Comparison of the Eulerian and Lagrangian methods for predicting particle transport in enclosed spaces. *Atmospheric Environment*. 41(25), pp. 5236-5248. https://doi.org/10.1016/j.atmosenv.2006.05.086